A&A 578, A103 (2015)
DOI: 10.1051/0004-6361/201525973

Astronomy & Astrophysics

The doubly eclipsing quintuple low-mass star system 1SWASP J093010.78+533859.5⋆

M. E. Lohr[1], A. J. Norton[1], E. Gillen[2], R. Busuttil[1], U. C. Kolb[1], S. Aigrain[2], A. McQuillan[2,3], S. T. Hodgkin[4], and E. González[5]

[1] Department of Physical Sciences, The Open University, Walton Hall, Milton Keynes MK7 6AA, UK
e-mail: Marcus.Lohr@open.ac.uk
[2] Sub-department of Astrophysics, Department of Physics, University of Oxford, Keble Road, Oxford OX1 3RH, UK
[3] School of Physics and Astronomy, Raymond and Beverly Sackler, Faculty of Exact Sciences, Tel Aviv University, 69978 Tel Aviv, Israel
[4] Institute of Astronomy, Madingley Road, Cambridge CB3 0HA, UK
[5] Observatori Astronómic de Mallorca, Camí de l'Observatori s/n, 07144 Costitx, Mallorca, Spain

Received 26 February 2015 / Accepted 17 April 2015

ABSTRACT

Our discovery of 1SWASP J093010.78+533859.5 as a probable doubly eclipsing quadruple system, containing a contact binary with $P \sim 0.23$ d and a detached binary with $P \sim 1.31$ d, was announced in 2013. Subsequently, Koo and collaborators confirmed the detached binary spectroscopically, and identified a fifth set of static spectral lines at its location, corresponding to an additional non-eclipsing component of the system. Here we present new spectroscopic and photometric observations, allowing confirmation of the contact binary and improved modelling of all four eclipsing components. The detached binary is found to contain components of masses 0.837 ± 0.008 and 0.674 ± 0.007 $M_\odot$, with radii of 0.832 ± 0.018 and 0.669 ± 0.018 $R_\odot$ and effective temperatures of 5185^{+25}_{-20} and 4325^{+20}_{-15} K, respectively; the contact system has masses 0.86 ± 0.02 and 0.341 ± 0.011 $M_\odot$, radii of 0.79 ± 0.04 and 0.52 ± 0.05 $R_\odot$, respectively, and a common effective temperature of 4700 ± 50 K. The fifth star is of similar temperature and spectral type to the primaries in the two binaries. Long-term photometric observations indicate the presence of a spot on one component of the detached binary, moving at an apparent rate of approximately one rotation every two years. Both binaries have consistent system velocities around -11 to -12 km s^{-1}, which match the average radial velocity of the fifth star; consistent distance estimates for both subsystems of $d = 78 \pm 3$ and $d = 73 \pm 4$ pc are also found, and, with some further assumptions, of $d = 83 \pm 9$ pc for the fifth star. These findings strongly support the claim that both binaries – and very probably all five stars – are gravitationally bound in a single system. The consistent angles of inclination found for the two binaries ($88.2 \pm 0.3°$and $86 \pm 4°$) may also indicate that they originally formed by fragmentation (around 9–10 Gyr ago) from a single protostellar disk, and subsequently remained in the same orbital plane.

Key words. stars: individual: 1SWASP J093010.78+533859.5 – binaries: close – binaries: eclipsing – binaries: spectroscopic

1. Introduction

During the course of a search for orbital period variations in short-period eclipsing binary candidates in the SuperWASP archive (Pollacco et al. 2006), described in Lohr et al. (2012, 2013b), several unusual systems of particular astronomical interest were encountered. Amongst these, 1SWASP J234401.81--212229.1, discussed in Lohr et al. (2013a) and Koen (2014), appears to be a triple system containing an M+M dwarf contact binary. Here we explore 1SWASP J093010.78+533859.5 (hereafter J093010), an apparent quintuple system containing two eclipsing binaries, one of only a handful of known doubly eclipsing multiples.

Higher-order multiple systems are of value in general for testing models of stellar formation and long-term dynamical stability. When they contain two double-lined spectroscopic and eclipsing binaries, they provide a highly unusual opportunity to determine the component stars' physical parameters and so to understand the structure and potential origins of the whole system.

2. Background

A near neighbour of J093010 (1SWASP J093012.84+533859.6, hereafter J093012) was identified as a candidate short-period eclipsing binary in Norton et al. (2011), and its orbital period confirmed in Lohr et al. (2012). However, in our subsequent more thorough search for eclipsing candidates, J093010 was identified as exhibiting the same period and light curve shape, but a higher mean flux and greater amplitude of flux variability; hence, it was regarded in Lohr et al. (2013b) as the probable true source of the observed eclipsing variation, with J093012 being a fainter near-duplicate light curve, falling within the same photometric aperture used by SuperWASP. At the location of J093012 there is a magnitude 18 source listed in the USNO-B1 catalogue, separated from J093010 by approximately 18″, which would not have been detectable by SuperWASP in its own right.

The eclipsing source's apparently significant period change, associated with an erratic O−C diagram, had been rejected initially as the result of contamination by a nearby star (Lohr et al. 2012), but in Lohr et al. (2013b) a fuller explanation was pursued. Prior to analysis, the data for J093010 and J093012 were combined to maximize the available observations. J093010's light curve, folded at 19 674.574 s, then showed a typical contact

⋆ Table 1 is available in electronic form at http://www.aanda.org

binary shape, but with significant non-Gaussian data scatter below the main curve. A visual examination of the object's full light curve suggested the cause was additional deep eclipses on certain individual nights, implying a second eclipsing body in the field of view. A frequency power spectrum also supported an additional periodic signal near 1.3 d. Subtracting the median binned light curve (corresponding to the contact binary) from the data revealed the light curve of an EA-type (detached) eclipsing binary with period 112 799.109 s.

The juxtaposition of these two binaries on the sky did not seem to be coincidental. Two sources had been observed at this location by HIPPARCOS as TYC 3807-759-1 and TYC 3807-759-2, with equivalent Johnson V magnitudes 9.851 and 10.990, respectively; a separation of 1.″88; and a proper motion of pmRA: –8.0 mas yr^{-1}, pmDE: –9.4 mas yr^{-1}, measured at their joint photocentre. The tiny angular separation and similar magnitudes favoured a plausible interpretation of the two eclipsing binary systems as being gravitationally bound in a quadruple doubly eclipsing system.

Only five other doubly eclipsing quadruple systems had been proposed at the time of our announcement of this discovery in Lohr et al. (2013b): BV Dra+BW Dra (Batten & Hardie 1965), V994 Her (Lee et al. 2008), OGLE-LMC-ECL-16545 (Graczyk et al. 2011), KIC 4247791 (Lehmann et al. 2012), and Cze V343 (Cagaš & Pejcha 2012). The contact binary in J093010 had a shorter period than any system in the other five quadruples, making it particularly amenable to further observations.

Koo et al. (2014) obtained BV photometry over several months in 2012–2013 for each eclipsing binary separately, and time-series spectra for the whole system. Their light curves made clear that the brighter signal (TYC 3807-759-1) was associated with the detached binary, and they consequently termed this source J093010A, and the fainter source J093010B (containing the contact binary). We follow this convention here. Although Koo et al. were unable to detect a spectral signature of the assumed contact binary in their combined spectra (due in part to the length of their exposures), they did observe clear line splitting and shifting with the period of the proposed detached binary, confirming its reality. They also unexpectedly detected an additional set of static spectral lines which they interpreted as a third component in J093010A, which would make the whole system a highly unusual doubly eclipsing quintuple.

Independently, we obtained time-series spectroscopy over three nights in 2012–2013 for J093010A and J093010B separately, and near-simultaneous RGB photometry for the whole system to help establish the phases of the observations. Our new data sets thus complement those provided in Koo et al. (2014), allowing us to model both binaries quite fully; the revisited SuperWASP observations also provide further long baseline information.

2.1. Spectroscopy

49 long-slit spectra were obtained by E. Gillen for J093010 on 22 and 31 December 2012, and on 2 January 2013, using the red arm of the ISIS spectrograph on the 4.2 m *William Herschel* Telescope at La Palma. The R1200R grating provided an intermediate resolution of 0.24 Å per pixel. A usable wavelength range of ~8350–9000 Å was obtained, to capture the Ca II triplet important in low-mass stars. Exposure lengths ranged from 5 to 360 s (see Table 1): short enough in all cases to avoid motion blur for the contact binary.

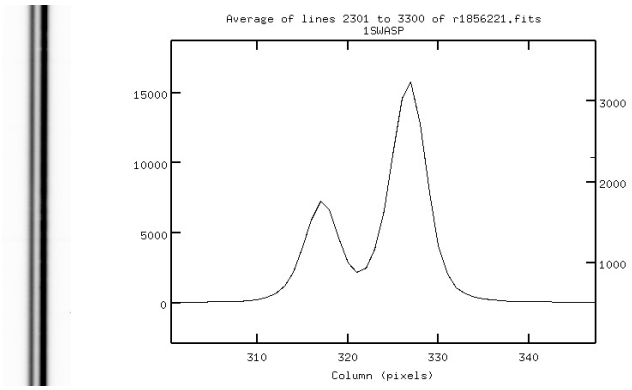

Fig. 1. *Left*: section of spectra for J093010A and J093010B from a single 360 s exposure, showing spatial separation. *Right*: plot of spectral profile from same exposure, cut perpendicular to the dispersion axis, showing two clear peaks in the line dispersion function. The stronger peak on the right hand side corresponds to J093010A.

The images were flat-fielded and bias-corrected by E. Gillen as part of a larger observing programme. On all but one image, two partially overlapping dispersion lines were clearly visible (e.g. Fig. 1), corresponding to J093010A and J093010B, and we were able to extract separate spectra for each, using standard IRAF tools and optimal extraction. Wavelength calibration was carried out using arc spectra taken with CuArNe lamps. Signal-to-noise ratios reached 340 for the brighter J093010A and 220 for the fainter J093010B in the longest exposures, when both systems were near quadrature, and fell to 45 and 25 respectively in the initial 5 s exposure.

Preliminary radial velocities were extracted using the IRAF task FXCOR, using a synthetic spectrum with T = 4500 K and log g = 4.5 as the comparison template. These allowed approximate determination of mass ratios and radial velocity curve amplitudes, which provided initial input parameters for spectral disentangling of J093010A and B. The KOREL code (Hadrava 2012), implemented on the Virtual Observatory[1], was used to disentangle sections of the spectra prepared with Hadrava's PREKOR software, giving improved values for mass ratio and radial velocities. The disentangled spectra were also compared with appropriately broadened template spectra extracted from the PHOENIX synthetic stellar library (Husser et al. 2013)[2], to estimate the temperatures of individual components.

2.2. Photometry

67 images of J093010 (55 each in Baader G and B filters, 57 in R) were taken with the Open University's robotic 0.425 m PIRATE telescope (Holmes et al. 2011; Kolb 2014) in Mallorca on the night of 30–31 December 2012, monitored by R. Busuttil. All exposures were 80 s; short enough to avoid phase smearing for the shorter-period system. Corrections for bias level, dark current and flat-fielding were made to the frames using standard IRAF tools, and four comparison stars were identified on the frames: TYC 3807-1509-1, TYC 3807-54-1, TYC 3807-1503-1 and TYC 3807-621-1. These had catalogue colours indicative of classes between late F and G, and V magnitudes between 9 and 10, similar to J093010. They were checked for short and long-term variability with their SuperWASP light curves, and did not exhibit significant variations. Aperture photometry was

[1] https://stelweb.asu.cas.cz/vo-korel
[2] phoenix.astro.physik.uni-goettingen.de

carried out on all the stars using the IRAF APPHOT package, and the light curves of the comparison stars were combined in IDL. Differential light curves were then obtained for J093010 relative to this combined comparison curve.

The SuperWASP archive data for J093010 were also reconsidered: there are 5964 photometric points in V, observed between October 2007 and April 2009. (The fainter duplicate object J093012 has 5950 points covering the same time span; its data were used here as a check on the results found for J093010.) For reference, SuperWASP exposure lengths are 30 s. Initial values for the orbital periods of the two eclipsing binaries were found with a custom IDL code described in Lohr et al. (2014b): 19 674.594 ± 0.005 s and 112 799.10 ± 0.15 s; then a second code was written to separate the two eclipsing signals. The light curve was first folded on the shorter period corresponding to the contact binary, and phase-binned to give a smooth mean curve (90 bins were used); an optimally-weighted average was then found for the data points in each bin (which corresponded closely to the visible contact binary signal). A spline curve was interpolated to these binned average points, and subtracted from the full light curve. The residue was then folded on the longer period corresponding to the detached binary, and a binned average curve obtained as before. This was again subtracted from the full light curve, to leave a clean contact binary light curve as output. This clean mean contact curve was subtracted a second time from the full data set, to leave a clean detached binary light curve for output. Our initial period-searching code was run again on the separated files, and its resulting period values were used to initialize the signal-separation code for a second iteration. This continued until convergence was reached for both periods.

The BV light curves of Koo et al. (2014) were also used in our modelling; most details of the photometry are given in that paper, though we add that the exposure lengths were below 25 s, avoiding any risk of phase-smearing for even the shorter-period binary.

3. Results

3.1. Orbital periods

The orbital periods based on SuperWASP data rapidly converged on 19 674.47 ± 0.03 s for the contact binary and 112 798.90 ± 0.16 s for the detached binary i.e. 0.2277138(3) d and 1.3055428(19) d respectively. (The periods for J093012 did not converge, but oscillated within the narrow ranges 19 674.43–19 674.52 and 112 798.9–112 800.0, which include and support the results for J093010.) These periods fall within the uncertainties of those found by Koo et al. from their photometry: 0.2277135(16) d and 1.30550(4) d, though their figure for the detached binary's period is based on a single measured primary eclipse time and three secondary eclipses.

No period change was detected within the SuperWASP data for either binary; extrapolating forward from the most precisely measured times of minimum for the SuperWASP data, using our periods, gives an O−C value of just −30 s for the Koo et al. primary minimum for the detached system, and ∼+200 s for their primary minima for the contact system. The small size of these discrepancies further supports both the absence of significant period change (especially in the detached system) and the reliability of our periods, calculated over long base lines using whole light curves, rather than minimum timings alone. We therefore prefer our periods for the remainder of the analysis, but use Koo et al.'s more precise and recent primary minimum timings to calculate phases.

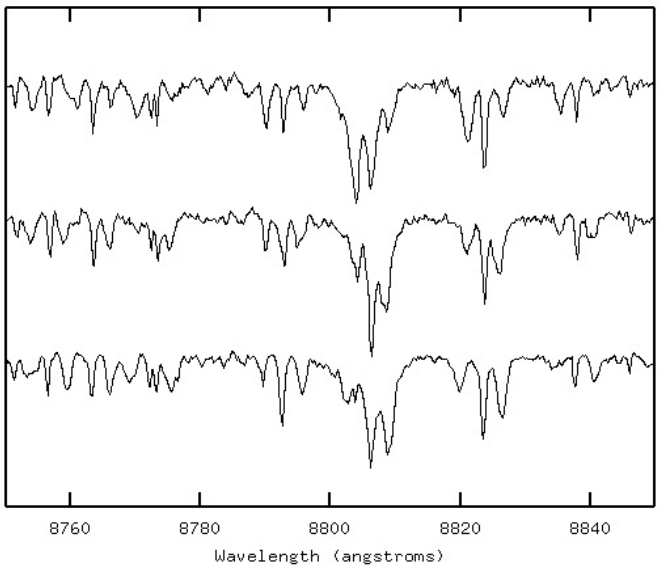

Fig. 2. Extract of WHT spectra for J093010A at approximate phases 0.16, 0.64 and 0.75 (top to bottom). Relatively isolated absorption lines at around 8793, 8806 and 8823 Å exhibit three-way splitting, with the outer pair also shifting between phases.

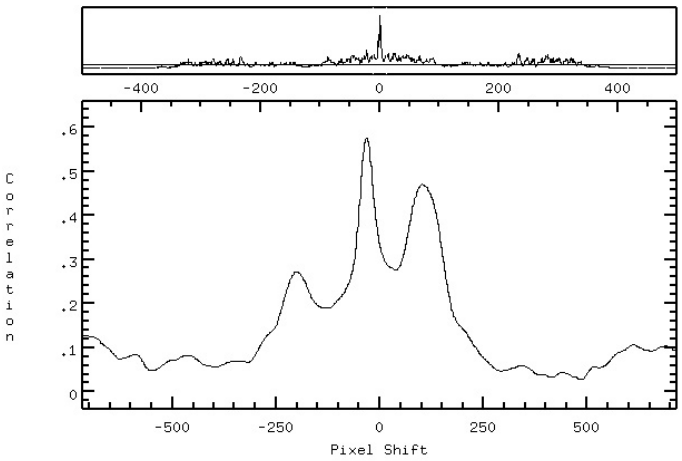

Fig. 3. Cross-correlation plot for J093010A at phase 0.75, exhibiting three strong peaks corresponding to three stellar components (primary on the right, secondary on the left, tertiary in the middle). The broadest absorption lines were excluded from the cross-correlation to minimize the radial velocity uncertainties.

3.2. Radial velocities and spectroscopic parameters

Koo et al. measured radial velocities for J093010A by fitting three Gaussians simultaneously to five isolated absorption lines in their spectra, in the range 6400–6800 Å. Our longer wavelength range contained such a profusion of blended lines that this approach would have been impossible; indeed, it was hard to detect three-way line splitting from visual examination of the spectra over most of the range (Fig. 2 illustrates a small region where the triplets are relatively isolated). However, cross-correlation revealed three extremely clear correlation peaks for every spectrum (e.g. Fig. 3), allowing preliminary radial velocities to be measured easily for the system.

Spectral disentangling was then achieved for three subregions of our spectra containing narrow and well-defined lines, and converged on consistent values for mass ratio

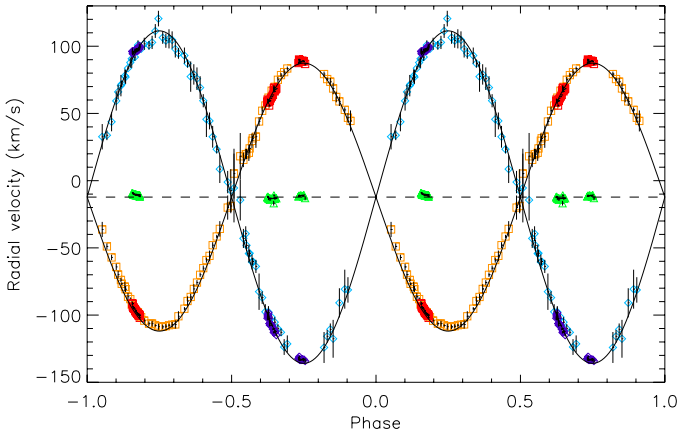

Fig. 4. Radial velocity curves for J093010A. The primary's measurements are indicated by squares, the secondary by diamonds and the third component by triangles. Data from Koo et al. (2014) is in fainter print (orange and light blue in the online version of the paper) and our new results are in bold print (red, dark blue and green). Phase-folding uses Koo et al.'s primary minimum time of HJD 2 456 346.78443 and our optimum period. PHOEBE model fits are overplotted (solid black curves) and the location of the modelled system velocity is shown by the dashed line.

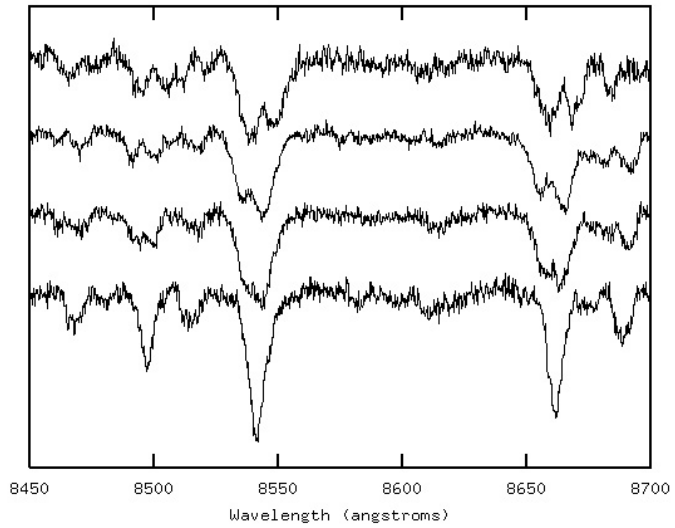

Fig. 5. Extract of WHT spectra for J093010B at approximate phases 0.24, 0.66, 0.88 and 0.99 (top to bottom). The Ca II triplet of absorption lines at around 8498, 8542 and 8662 Å exhibit clear splitting and shifting between phases.

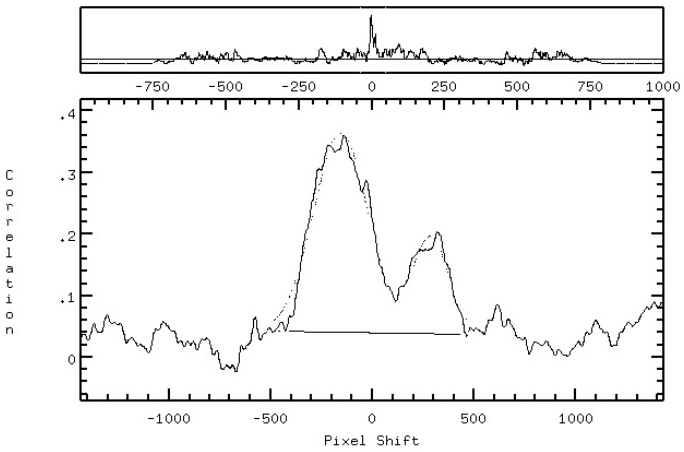

Fig. 6. Cross-correlation plot for J093010B at phase 0.24, exhibiting two strong peaks corresponding to the binary components (primary on the left, secondary on the right). The two broadest calcium lines at 8542 and 8662 Å were excluded from the cross-correlation to minimize the uncertainty in the radial velocity measurements.

($q = 0.806 \pm 0.007$) and semi-amplitude of the primary's radial velocity curve ($K_1 = 99.4 \pm 0.7$ km s^{-1}). The resulting radial velocities were corrected to heliocentric values by disentangling telluric lines observed in the region 8250–8320 Å, and are given in Table 1. (These are very close to those found by the cross-correlation method, but with smaller uncertainties.) Figure 4 shows our results, together with those of Koo et al.: where our observations overlap with theirs (around phases 0.15 and 0.65) there is close agreement in both the amplitudes and absolute values of the curves; we have also fortuitously been able to observe the system around its secondary maximum (phase 0.75) where Koo et al. had a gap.

Also notable is our confirmation of the third strong and near-static component of the detached system spectra: Koo et al.'s fifth star. Since we have obtained separate spectra for J093010A and J093010B, we can be certain that this additional source occurs at the same location on the sky as the detached eclipsing binary, rather than being near the contact system or mid-way between the two. There is also very good reason to regard it as part of a gravitationally bound system including the detached binary: its radial velocities (average -11.6 ± 1.5 km s^{-1}) are visibly very close to the cross-over system velocity of the binary (modelled as -12.3 ± 0.2 km s^{-1}). While longer-term radial velocity and astrometry measurements would be required to demonstrate convincingly that the fifth star forms a triple subsystem with the detached binary (rather than, for example, the two binaries being more closely bound to each other), the coincidence of its spectrum with that of the binary in J093010A (see Fig. 1) makes this a more plausible hierarchy.

We were also able to measure radial velocities from most of the spectra for the candidate contact system in J093010B. Here, splitting and shifting of the strongest lines (primarily the Ca II triplet) was apparent from visual inspection of the spectra alone (e.g. Fig. 5), confirming this system as a double-lined spectroscopic binary also. The results from cross-correlation (e.g. Fig. 6) again provided starting values for spectral disentangling, and here we were able to disentangle the full spectrum as a single region, giving much smoother radial velocity curves with much smaller uncertainties than had been achieved by cross-correlation (Table 1). A mass ratio of 0.397 ± 0.006 and $K_1 = 105.1 \pm 1.3$ km s^{-1} were converged upon by disentangling; a slightly different value of reference minimum was also implied by the spectra: HJD 2 456 288.87687, where Koo et al.'s nearest minimum (based on photometry) was HJD 2 456 288.87879.

Our results are shown in Fig. 7: we have managed to capture the system around its primary maximum (phase 0.25) and on each side of its secondary maximum (near phases 0.6 and 0.9), giving sufficient phase coverage for decent modelling (though further observations around phases 0.4 and 0.75 would still be desirable). The cross-over velocity of the two curves is -11.3 ± 0.7 km s^{-1}: very close to the detached binary system velocity and the third component velocity in J093010A, strongly supporting the hypothesis that the two binaries and the fifth star are gravitationally bound within a quintuple system with a common motion relative to the Sun.

The disentangled spectrum for the primary component of J093010B was best fitted by a PHOENIX synthetic template

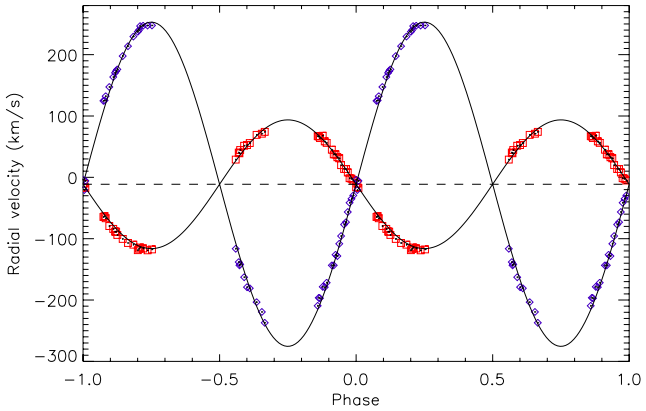

Fig. 7. Radial velocity curves for J093010B, based on our WHT observations. The primary is shown with red squares and the secondary with blue diamonds; uncertainties are generally smaller than the symbol size. Phase-folding uses HJD 2 456 288.8780, found by PHOEBE modelling of radial velocity and light curves simultaneously, and our optimum period. The dashed line shows the location of the (modelled) system velocity.

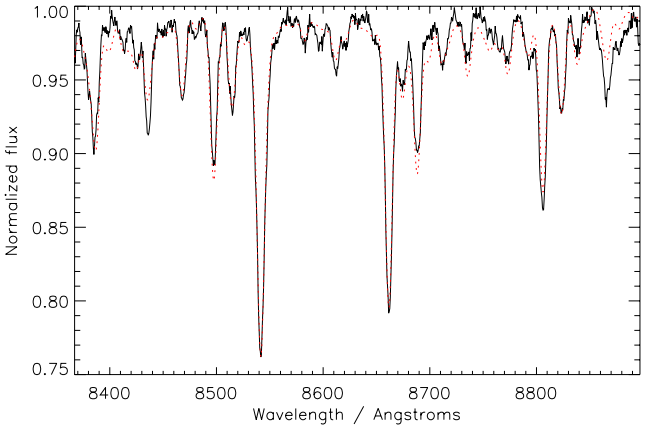

Fig. 8. Disentangled renormalized spectrum for primary component of J093010B (black solid lines), with best-fitting PHOENIX synthetic template overplotted (red dotted lines). The prominent absorption lines are Ca II, Mg I, Fe I, Ti I and Al I.

with $T = 4700 \pm 50$ K and $\log g = 4.5$ (Fig. 8). The secondary component's spectrum was of very similar shape, but had far lower signal-to-noise ratio and so was not used to assess the common temperature of the contact binary. The temperature found here spectroscopically is entirely consistent with that suggested by Koo et al.'s $B - V$ colour for J093010B during secondary eclipse i.e. 4680 ± 50 K.

The three components of J093010A were difficult to disentangle convincingly owing to heavy blending of strong lines and our rather limited phase coverage; however, a reasonably good fit to the tertiary component was achieved, since it exhibited narrower, deeper lines than the detached binary components, presumably owing to greater rotational broadening in the latter. Templates with $T = 5100 \pm 200$ K and $\log g = 4.5$ (Fig. 9) provided the best matches, suggesting an early K spectral type for this star. Measurements of the equivalent widths of several distinct triplets of lines in the original spectra also indicated that the primary's lines were somewhat stronger than those of the tertiary, which could imply a slightly higher temperature (and

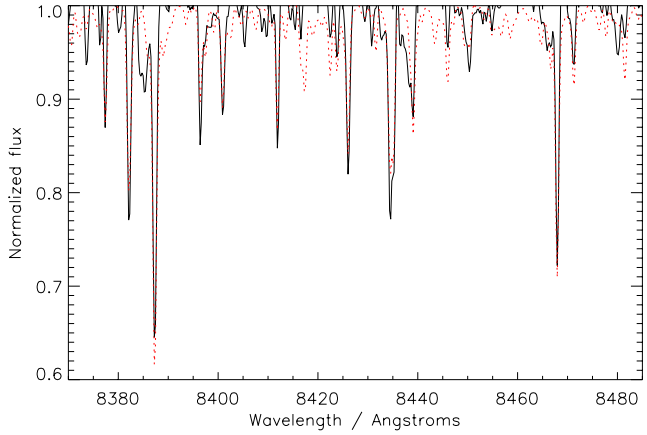

Fig. 9. Part of disentangled renormalized spectrum for tertiary component of J093010A (see caption to Fig. 8).

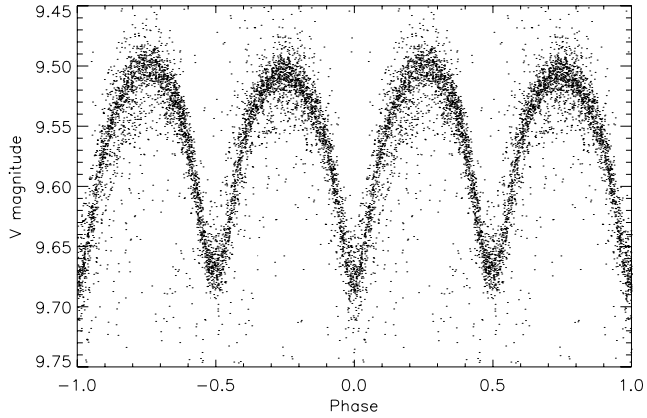

Fig. 10. SuperWASP folded light curve for J093010B, converted to V magnitudes. The maximum magnitude is that of the quintuple system as a whole.

mass). Spectroscopy with better phase coverage would be desirable in future to allow direct determination of the temperatures of all three components in J093010A. However, we were able to estimate temperatures for the detached binary components from the photometry, during the modelling process described in Sect. 4.

3.3. Light curve characteristics

Moving to the photometric results, we can compare the light curves obtained by Koo et al. (2014) for J093010A and B separately with the SuperWASP light curves extracted from the combined light variation for the whole system. In each case, the SuperWASP amplitudes are smaller, and the magnitudes lower, because there is an effective third light included containing the (maximum) contributions from the other three stars. For the contact binary the SuperWASP curve (Fig. 10) is evidently the same general shape as the BV curves (Fig. 2 in Koo et al.): the secondary eclipses are visibly flat-bottomed with the primary minimum fractionally deeper than the secondary; the secondary maximum is also slightly lower than that of the primary, though this effect is perhaps stronger in Koo et al.'s curves, which would support the presence of a long-term static spot on one of the components.

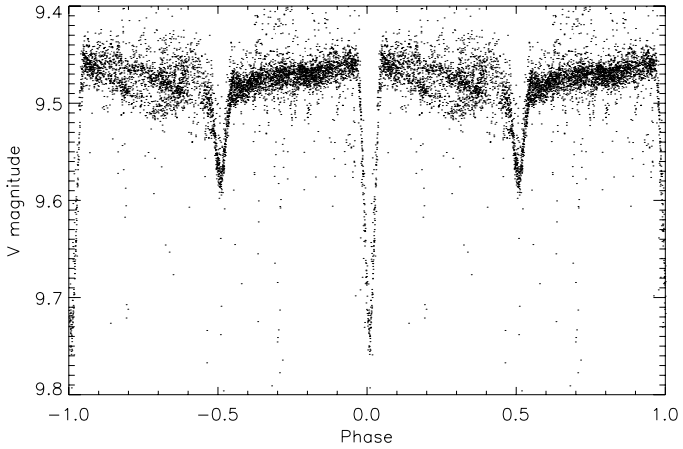

Fig. 11. SuperWASP folded light curve for the detected binary in J093010A, converted to *V* magnitudes. The maximum magnitude is that of the quintuple system as a whole.

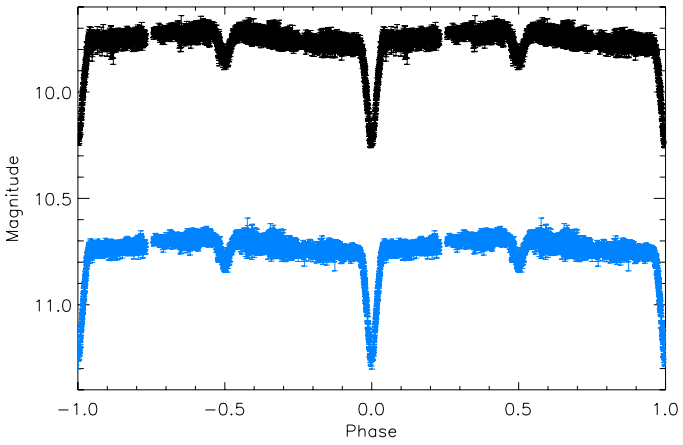

Fig. 12. Koo et al. light curves for the detached binary in J093010A, in *V* (top) and *B* (bottom), converted from differential instrumental magnitudes to standard magnitudes using normalization indices provided in Koo et al. (their Table 6).

For the detached binary light curves in J093010A (Figs. 11 and 12), the relative depths of the two eclipses are comparable in the SuperWASP data and Koo et al.'s data, and together with the sharp ingresses and egresses of the eclipses they support a well-detached EA-type system. The eclipses are equally spaced and of the same duration, indicating no significant orbital eccentricity. The primary eclipse appears flat-bottomed while the secondary eclipse's shape is arguably more curved; if taken at face value this would suggest that the secondary's radius is (surprisingly) greater than that of the primary. The out-of-eclipse region would be expected to be essentially flat in an EA-type light curve, but is not. In the SuperWASP curve, the region between phases 0.1 and 0.4 is far more scattered and noisy than the region between phases 0.6 and 0.9; moreover, the maximum is near the primary minimum, while it occurs just before the secondary minimum in Koo et al.'s curves; they suggest that this latter feature results from a moving spot on one of the components.

To explore this idea further, we split up the SuperWASP detached binary curve by time, into three sections of contiguous data covering several months. The profile of the out-of-eclipse region clearly changed over time, with its minimum occurring around phase 0.8 near HJD 2 454 510, phase 0.4 near HJD 2 454 820 and phase 0.3 near HJD 2 454 870 i.e. apparently moving negatively in phase at a rate of (very) roughly one cycle every two years. The superposition of these three (fairly smooth) curves produced the apparent scatter in the curve of Fig. 11. The most plausible explanation for this moving profile would indeed seem to be a spot on the surface of one of the detached system components, rotating at a slightly different rate from the star as a whole, perhaps because of differential rotation.

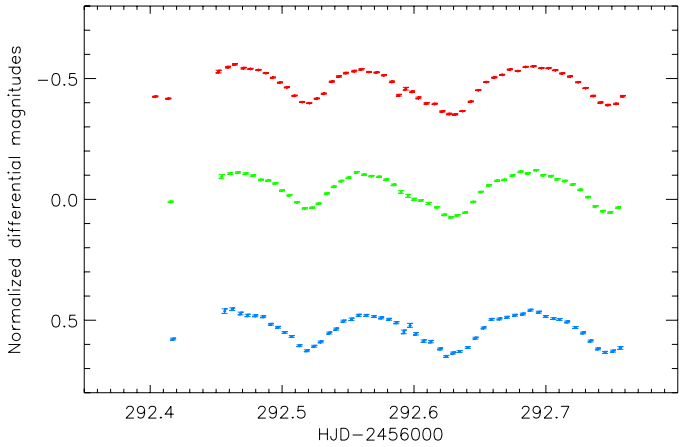

Fig. 13. Normalized differential PIRATE light curves for J093010 in Baader *R* (red, top), *G* (green, middle) and *B* (blue, bottom) filters.

Finally, Fig. 13 shows the PIRATE *RGB* photometry obtained for the whole system during one night. As predicted by the SuperWASP ephemeris, contact binary primary minima occur around HJD 2 456 292.519 and 2 456 292.748, while the two eclipsing systems' secondary minima overlap in between (this is most clearly seen in the *G* curve, where the detached system secondary minimum occurs around HJD 2456292.60 and the contact one around HJD 2 456 292.63). The second night of our WHT spectra begins just as this photometry ends, and covers phases ∼0.07−0.25 of the contact system, which is entirely consistent with the light curve. Additional nights of photometry would be useful to establish the average shapes of the three-colour light curves; however, we note that the three curves have very similar shapes. The primary eclipses of J093010B are perhaps fractionally deeper in *B* than *R*, with *G* intermediate. Similarly, Koo et al.'s standardized *BV* magnitudes for J093010A indicate that the primary eclipses are deeper in *B*, while the secondary eclipses are deeper in *V* i.e. the primary is hotter than the average of J093010A's three components, while the secondary is cooler.

3.4. Flux contributions

We can make further estimates of the relative flux contributions of the five stars from the photometry and spectroscopy. Starting with the SuperWASP light curves in SuperWASP flux units, if we assume that J093010A and J093010B's angles of inclination are close to 90° (since both systems contain flat-bottomed eclipses supporting near-totality), the depth of each component's eclipse gives a minimum value for its flux contribution (J093010A primary: 38, secondary: 15; J093010B primary: 25, secondary: 23). Adding these four fluxes and subtracting them from the total flux (160) when no component is eclipsed gives us a maximum flux estimate for the fifth component (59). These values would suggest that the tertiary makes up at most 53% of the flux in J093010A (in *V*), and the primary and

secondary at least 34% and 13% respectively. Koo et al.'s V band data similarly supports contributions of around 53%, 37% and 10% respectively, using the same approach; in B the proportions are 53%, 40% and 8%.

Furthermore, the SuperWASP fluxes allow us to estimate J093010B:J093010A flux contributions at the former's maximum and primary minimum as 43% and 21%. These figures can be compared with the spectroscopic fluxes, found from fits to the continua of the extracted spectra, evaluated at 8500 Å and scaled to account for the different exposure lengths: near the maxima of both systems (phase 0.75 of J093010A and 0.63 of J093010B) the ratio is 44%, and near contact primary minimum (around phase 0.18 of J093010A and 0.0 of J093010B) it is 24%, showing considerable similarity across optical and near-infrared observations. These consistent estimates provide a starting point for further modelling of the five stars.

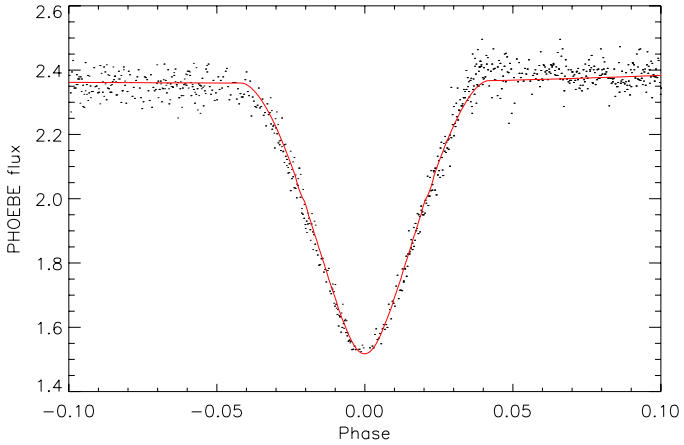

Fig. 14. PHOEBE best model fit (red solid curve) to primary eclipse of J093010A in V, showing good match to eclipse width, shape and depth.

4. Modelling and discussion

To determine parameters for the eclipsing components of J093010, the two binaries were modelled separately using the PHOEBE software (Prša & Zwitter 2005), built upon the code of Wilson & Devinney (1971).

The starting assumptions for J093010A, based on its light curve, were that it is a detached binary in a circular orbit viewed nearly edge-on, with $M_1 > M_2$, $T_1 > T_2$, a third light contributing up to half the total flux, and a spot on one component. The mass ratio ($q = 0.806$, where Koo et al. (2014) had found 0.841 by modelling) found from spectral disentangling was set as a non-adjustable parameter; the period was also fixed at 1.3055428 d (from the SuperWASP results) and the reference HJD_0 at 2 456 346.78443 (from Koo et al.'s single primary minimum timing); data was not binned or converted to phases prior to modelling. With the angle of inclination i set to 90°, the radial velocity curves were first fitted for $a \sin i$ (a proxy to the semi-major axis) and system velocity γ_0 simultaneously, and the optimum values found were not adjusted subsequently, since light curves are largely insensitive to these parameters.

Figure 4 shows the best fit obtained for the combination of our radial velocity data and that of Koo et al.. Similar results were found when modelling our data sets separately: $a \sin i$ of $5.765 \pm 0.014\ R_\odot$ and $5.607 \pm 0.014\ R_\odot$ for us and them respectively; and γ_0 of -12.3 ± 0.2 km s^{-1} and -10.4 ± 0.2 km s^{-1}. Combining the data sets reduced the formal uncertainties on the two parameters in comparison with each data set considered alone ($a \sin i = 5.759 \pm 0.010\ R_\odot$ and $\gamma_0 = -12.24 \pm 0.17$ km s^{-1}), and this combination of radial velocity data was used for the remainder of the modelling.

To model Koo et al.'s light curves, a valid third light contribution needed to be included, more precise than the <53% estimated above. While Koo et al. seem to have fitted their curves treating third light as a free parameter, we feared there might be strong correlations between this and other fitted parameters, and so sought to constrain the value of the third light independently. Since the eclipses of J093010A appear total-annular, we could determine the phases of first, second, third and fourth contact ($\phi_{1,2,3,4}$) quite precisely for the primary eclipse (see Fig. 14), using Koo et al.'s BV photometry, and then estimate the radii using these formulae from Hilditch (2001):

$$(\phi_2 - \phi_1) = (\phi_4 - \phi_3) = \frac{2R_2}{2\pi a} \quad (1)$$

$$(\phi_3 - \phi_1) = (\phi_4 - \phi_2) = \frac{2R_1}{2\pi a}. \quad (2)$$

On the assumption that the primary had the larger radius, this gave $R_1 = 0.832 \pm 0.018\ R_\odot$ and $R_2 = 0.669 \pm 0.018\ R_\odot$ (where Koo et al. found $R_1 = 0.757 \pm 0.008\ R_\odot$ and $R_2 = 0.743 \pm 0.010\ R_\odot$). Then, we made use of an eclipse modelling guideline from Wilson (1994): "the ratio of the depth of the annular eclipse to the light remaining in the total eclipse is approximately the square of the ratio of smaller to larger star radii". We measured the depth of the annular (primary) eclipse in V and B (in PHOEBE flux units) from the light curves, and combined this with the ratio $(\frac{R_2}{R_1})^2$ to estimate the flux which would remain in the total (secondary) eclipse, if there were no third light contribution: this would be the true contribution of the primary star (1.33 ± 0.09 units in V and 0.56 ± 0.04 units in B). The secondary's flux was given directly – and hence with greater precision – as the depth of the total eclipse (0.275 ± 0.011 units in V and 0.090 ± 0.007 in B). By subtracting the primary and secondary fluxes from the maximum flux in the light curves, the tertiary's contribution could then be estimated more precisely (0.90 ± 0.09 units in V and 0.37 ± 0.04 in B) as 36% ± 4: somewhat larger than the fitted values found by Koo et al. of 31% in V and 32% in B. These values for third light were then fixed for the rest of the modelling.

The Kopal potentials $\Omega_{1,2}$ for the two eclipsing stars were then set to values which would reproduce the radii determined above (7.74 and 8.04 respectively), indicating strongly negative filling factors, as expected for a well-detached system. These values gave excellent matches to the widths of the eclipses (e.g. Fig. 14). The effective temperatures of both components were also estimated from their $B - V$ colours, using the individual fluxes found above: these were 4970^{+240}_{-210} K for the primary and 4470 ± 160 K for the better-determined secondary (by the same method, the third component was estimated to have $T_3 = 4900^{+370}_{-310}$, consistent with the value found from its disentangled spectrum earlier). Using these values for T_1 and T_2 gave a model which had too shallow a primary eclipse and too deep a secondary eclipse; their ratio was therefore increased by increments until both eclipses were equally well reproduced: this occurred at $T_1 = 5185$ K and $T_2 = 4325$ K. The angle of inclination i also required a slight decrease from 90° to match the depths of both eclipses simultaneously (hence a and $\Omega_{1,2}$ were also fractionally adjusted). As a further check on these temperatures, we may note that the ratio of primary to secondary eclipse depths matched the corresponding ratio of the stars' surface brightnesses, as would be expected (Wilson 1994).

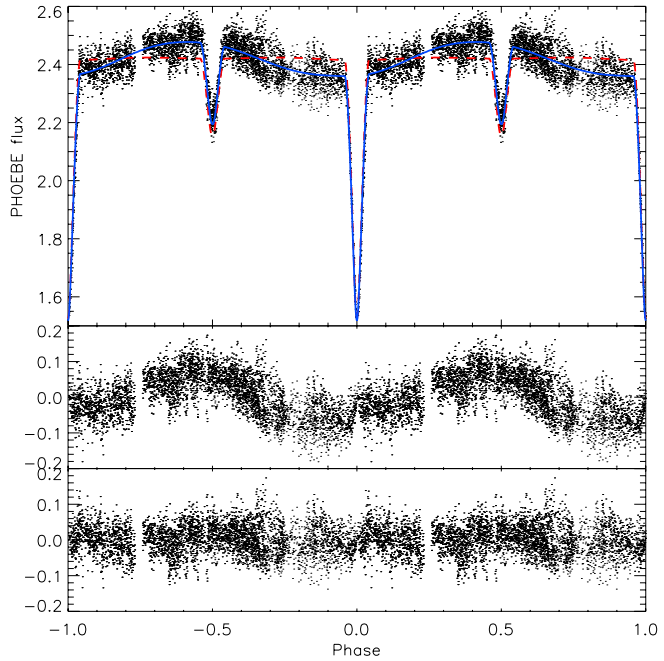

Fig. 15. *Top*: V band light curves for J093010A (data from Koo et al. 2014) expressed in PHOEBE flux units, with best-fitting PHOEBE model curves overplotted (dashed red lines indicate model with no spot, solid blue lines indicate one-spot example model). *Middle*: residuals from no-spot model, showing out-of-eclipse semi-sinusoidal light variation unaccounted for. *Bottom*: residuals from one-spot model, largely correcting for these variations.

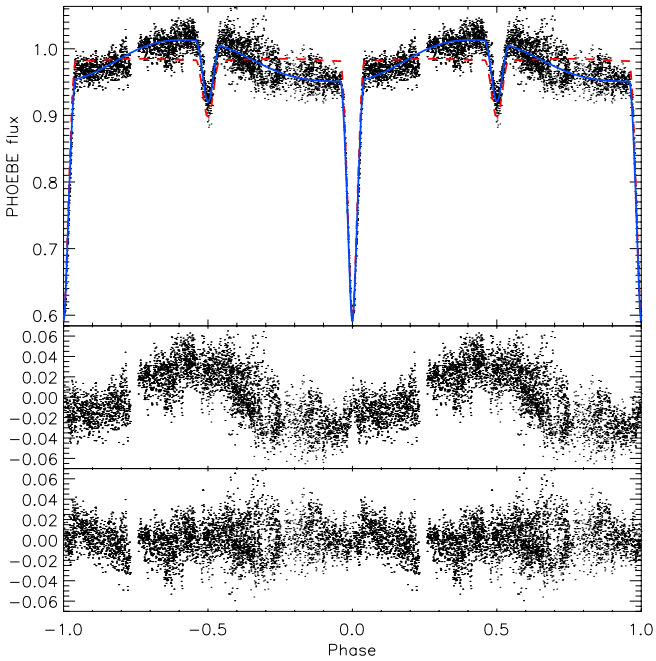

Fig. 16. B band light curves, fits and residuals for no-spot and one-spot models for J093010A (see caption to Fig. 15).

Fig. 17. Best-fit PHOEBE one-spot model for J093010A at phase 0.25. The large cool spot is visible on one limb of the (smaller) primary at quadrature.

As noted earlier, the apparently flat-bottomed primary eclipse could alternatively suggest $R_2 > R_1$, and so this possibility was also explored in the modelling. Using Eqs. (1) and (2) with the roles of R_1 and R_2 reversed, the components' radii, third light contribution, $\Omega_{1,2}$ and temperatures were again estimated as described above; however, no appropriate ratio of temperatures could be found which would fit both eclipse depths unless the uncertainties on $T_{1,2}$ were exceeded. Moreover, the best fit produced an inconsistency between the eclipse depth ratio and the surface brightness ratio. In view of these problems, and the mass-radius mismatch (which would be challenging to explain in a well-detached system), we prefer the original model for the remainder of the analysis. However, improved photometry, especially of the primary eclipse, would be desirable in future to confirm it more fully.

The full optimal light curve fits and their residuals are shown in Figs. 15 and 16. It is apparent that, while the eclipses are very well-fitted by this model, the out-of-eclipse portions are poorly fitted (reduced $\chi^2 = 17.1$ in V, 2.62 in B). This is almost certainly due to the presence of the assumed moving spot discussed earlier. To test this explanation, a single large cool spot was placed on the primary and its four parameters varied manually until a fair match to the light curve was achieved (colatitude 90°, longitude 29°, radius 95°and temperature 0.9835 × mean primary temperature). The resulting light curve fits and residuals are also shown in Figs. 15 and 16, and an image of the model system in Fig. 17. These models reproduce the light variations much better ($\chi^2 = 8.86$ in V, 1.18 in B).

It should be emphasized that we do not regard this as the only possible spot configuration which would reproduce the observed light curve variations: a cool spot on the opposite side of the secondary also works passably well, and hot spots on either component would also achieve similar results. Koo et al. used two cool spots with quite different parameters from ours, one on each component in their preferred model, to achieve a very close fit to the light curve; however, by appropriate placement of multiple spots, any light curve features whatsoever can be reproduced, and we did not wish to include more components in our model than were justifiable. That said, it is very likely that there are multiple spots on this system, or non-circular spots, whose modelling would produce an even better fit to the light curve, but a method such as Doppler tomography would be required to determine their nature more rigorously.

Table 2 gives the final parameters determined for J093010A, using the no-spot model (there is almost no change to any of these under the one-spot model). The uncertainties on a, γ_0 and i are formal errors generated by PHOEBE; the uncertainties on q, $T_{1,2}$, $R_{1,2}$ and $\Omega_{1,2}$ were obtained from independent measurements as described above; and the uncertainties on $M_{1,2}$ were found using the formula prescribed in the PHOEBE manual:

$$\sigma_{M_1} = M_1\left(3\frac{\sigma_a}{a} + 2\frac{\sigma_P}{P} + \frac{\sigma_q}{q+1}\right) \quad (3)$$

$$\sigma_{M_2} = M_2\left(3\frac{\sigma_a}{a} + 2\frac{\sigma_P}{P} + \frac{\sigma_q}{q(q+1)}\right). \quad (4)$$

J093010B was simpler to model. We started with the assumptions that it is a contact system (i.e. $T_1 = T_2 = 4700$ K, $\Omega_1 = \Omega_2$) in a circular orbit seen nearly edge-on, with $M_1 > M_2$,

Table 2. System and stellar component parameters for J093010A.

	Primary	Secondary
Orbital period (s)	112 798.90 ± 0.16	
Semi-major axis ($R_\odot$)	5.762 ± 0.010	
Mass ratio	0.806 ± 0.007	
System velocity (km s^{-1})	−12.24 ± 0.17	
Angle of inclination (°)	88.2 ± 0.3	
Kopal potential	7.74 ± 0.15	8.04 ± 0.18
Filling factor	−9.4	−10.0
Mass ($M_\odot$)	0.837 ± 0.008	0.674 ± 0.007
Radius ($R_\odot$)	0.832 ± 0.018	0.669 ± 0.018
Temperature (K)	5185^{+25}_{-20}	4325^{+20}_{-15}
Surface gravity	4.52	4.62
Bolometric luminosity	5.66 ± 0.02	6.92 ± 0.02
Flux contribution (V)	0.532 ± 0.036	0.110 ± 0.004
Flux contribution (B)	0.552 ± 0.040	0.089 ± 0.007

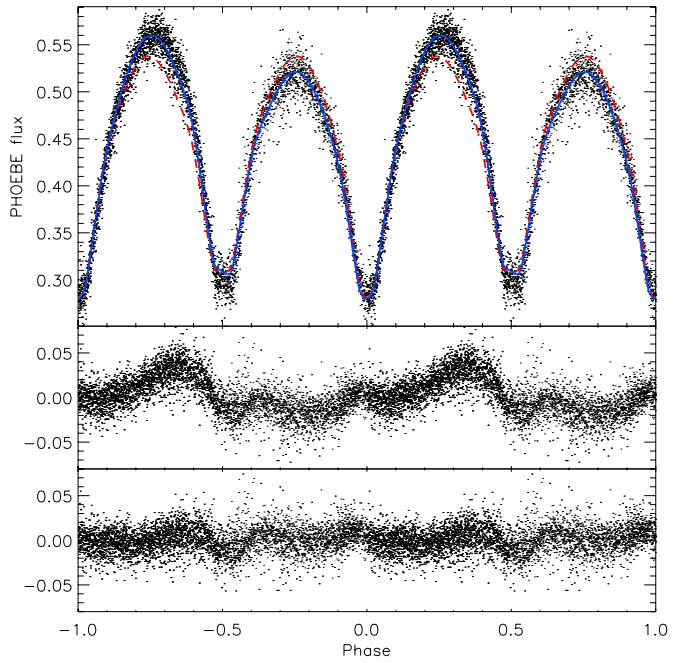

Fig. 18. V band light curves, fits and residuals for no-spot and one-spot models for J093010B (see caption to Fig. 15).

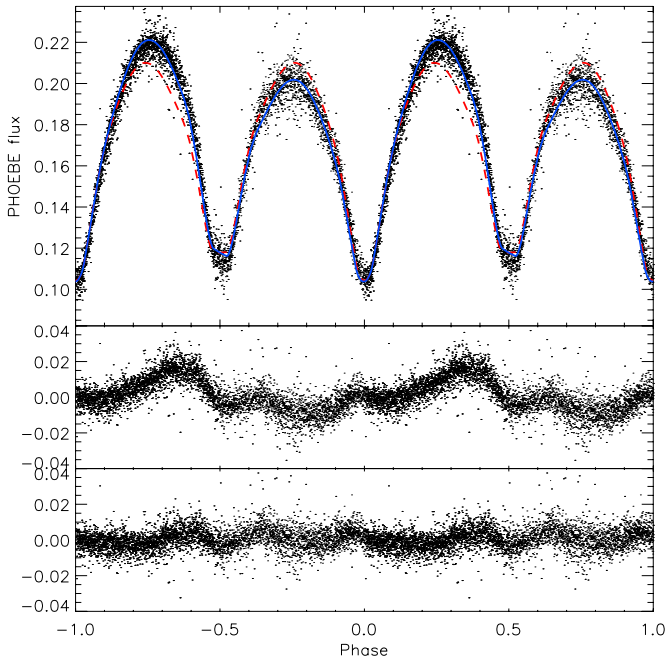

Fig. 19. B band light curves, fits and residuals for no-spot and one-spot models for J093010B (see caption to Fig. 15).

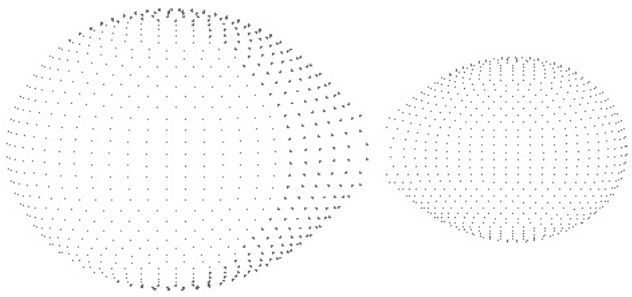

Fig. 20. Best-fit PHOEBE one-spot model for J093010B at phase 0.25. The large cool spot is visible at the limb of the (larger) primary.

$R_1 > R_2$ and no third light. The period was set to 0.2277138 d, the mass ratio to 0.397 ± 0.006, and the reference HJD_0 to 2 456 288.8780 (an average of the preferred values for radial velocity curves and light curves, since the continuous variation of J093010B's light curves made estimation of the time of primary minimum less reliable from photometry alone). We first fitted the radial velocity curves alone for $a \sin i$ and γ_0, as we did for J093010A, and found the best fit shown in Fig. 7, which gave $a \sin i = 1.661 \pm 0.009\, R_\odot$ and $\gamma_0 = -11.3 \pm 0.7$ km s^{-1}. Here, we note that Koo et al. (2014) also advanced a model for J093010B based purely on its light curve, which used a value for the mass ratio of 0.468 ± 0.005 found via the "q-search" method: some distance from the value found here.

Then, using Koo et al.'s BV light curves, and again adjusting a manually to keep $a \sin i$ at the value found earlier, i and Ω were allowed to reach their optima simultaneously (the continuous variation of the light curve meant that the approach taken to find J093010A's radii was impossible here). The best fits are shown in Figs. 18 and 19. The Kopal potential corresponding to this fit (2.63 ± 0.08) indicates a positive filling factor of 0.19 as expected for a contact system. The angle of inclination found is 86 ± 4°, which we note is consistent with that found for J093010A, suggesting that the two binaries may share an orbital plane and perhaps originally fragmented out of a single protostellar disk. However, measurements of the longitude of the ascending node for both binaries would be required to prove a common plane.

Again, a better fit can be achieved if a spot is modelled, to account for the different heights of the maxima. An example spotted model is shown in Figs. 18 to 20; this uses a spot on the primary with colatitude 90°, longitude 60°, radius 110°and temperature 0.979 × mean primary temperature. As with J093010A, we emphasize that this is only one of several possible ways to model the light variations using a single spot; Koo et al. used a cool spot on the primary and a hot spot on the secondary instead. Our resulting parameters for the system, shown in Table 3, are not affected by the presence of the spot. The uncertainties on a, q, γ_0, i and $M_{1,2}$ were found as for J093010A; that for T was estimated from the fitting to the disentangled primary spectrum; that for Ω is a formal output of PHOEBE; and those for $R_{1,2}$ were found by setting a, q and Ω to their extrema in appropriate

Table 3. System and stellar component parameters for J093010B.

	Primary	Secondary
Orbital period (s)	19 674.47 ± 0.03	
Semi-major axis ($R_\odot$)	1.665 ± 0.012	
Mass ratio	0.397 ± 0.006	
System velocity (km s^{-1})	−11.3 ± 0.7	
Angle of incl. (°)	86 ± 4	
Kopal potential	2.63 ± 0.08	
Filling factor	0.17	
Mass ($M_\odot$)	0.86 ± 0.02	0.341 ± 0.011
Radius ($R_\odot$)	0.79 ± 0.04	0.52 ± 0.05
Temperature (K)	4700 ± 50	
Surface gravity	4.58	4.53
Bolometric luminosity	6.20 ± 0.05	7.12 ± 0.05

combinations, which may be expected to overestimate these errors somewhat.

For both systems, distances were estimated by a similar method to that outlined in Koo et al.: absolute bolometric magnitudes (outputs from PHOEBE) were converted to absolute V magnitudes using bolometric corrections as tabulated in Flower (1996), and then combined using the formula (Hilditch 2001)

$$M_{V,\mathrm{total}} - M_{V,2} = -2.5 \log_{10}\left(1 + 10^{-0.4(M_{V,1} - M_{V,2})}\right). \quad (5)$$

Apparent V magnitudes of the maximum brightness of the system were determined from Koo et al.'s V light curves at their maxima for J093010B; for J093010A the contribution of the third star had to be removed first, using the component light ratios obtained during analysis. The formula (Hilditch 2001):

$$V - A_V - M_{V,\mathrm{total}} = 5 \log_{10} d - 5 \quad (6)$$

was then used to obtain distance estimates in parsecs (taking $A_V = 0.03$). For J093010A, $d = 78 \pm 3$ pc was found, and for J093010B, $d = 73 \pm 4$ pc; the ranges overlap substantially at 75−77 pc. Koo et al. found a consistent, if more uncertain value for J093010B of 77 ± 9 pc, but a shorter distance of 66 ± 7 pc for J093010A, probably due in the main to their handling of the third star's contribution to system light. The similarity of our distance estimates lends further support to the reality of the association between the two binaries.

An approximate distance was also estimated for the fifth star: its apparent V magnitude was found similarly to those for the binaries, from its fractional light contribution to J093010A and from the V light curves of Koo et al. Its absolute V magnitude was assumed to be that of a typical mid-main-sequence star with solar metallicity and $T = 5000 \pm 100$ K (combining the two independent effective temperature measurements obtained earlier), and was taken from Dartmouth stellar evolution models (Dotter et al. 2008)[3]. The formula above then gave $d = 81^{+9}_{-8}$ pc for a 5 Gyr star, or $d = 83 \pm 9$ pc for 10 Gyr; both ranges are consistent with the 75–77 pc distance estimate found for the two binaries. Although less reliable than the binary distances, this finding adds some support to the claim that the fifth star is physically associated with J093010.

The parameters for J093010A are fully consistent with Dartmouth models. Plotting temperature against luminosity, each binary component overlaps with the range of values expected for a star of its mass, assuming solar metallicity (Figs. 21 and 22). A very tiny negative value of [Fe/H] is perhaps implied for each, but nothing like the −0.25 found by Koo et al.

[3] http://stellar.dartmouth.edu/models/

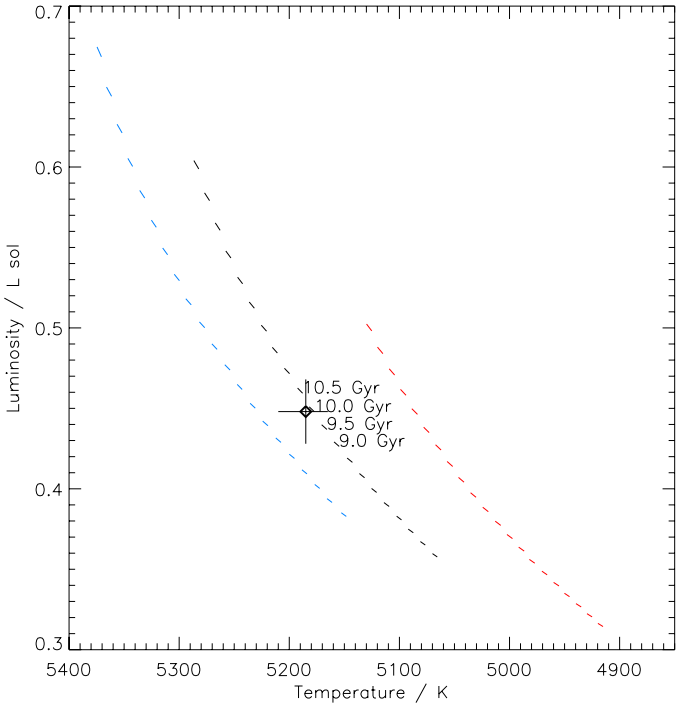

Fig. 21. Temperature-luminosity plot for primary of J093010A binary, compared with Dartmouth stellar evolution model isochrones. Each short curved line is a section of a model isochrone corresponding to masses between 0.829 and 0.845 $M_\odot$ i.e. the range of likely masses found from our modelling. The sections in the middle (black) have solar metallicity; those on the right (red) have [Fe/H] = 0.2 and those on the left (blue) have [Fe/H] = −0.05. Ages of four isochrones consistent with the primary's parameters are indicated.

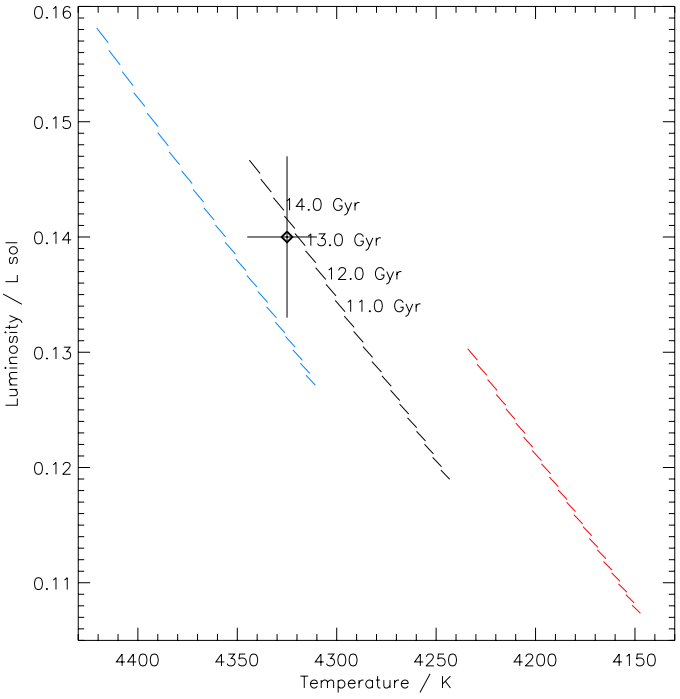

Fig. 22. Temperature-luminosity plot for secondary of J093010A binary, compared with sections of model isochrones corresponding to masses between 0.667 and 0.681 $M_\odot$ (see caption to Fig. 21 for further explanation).

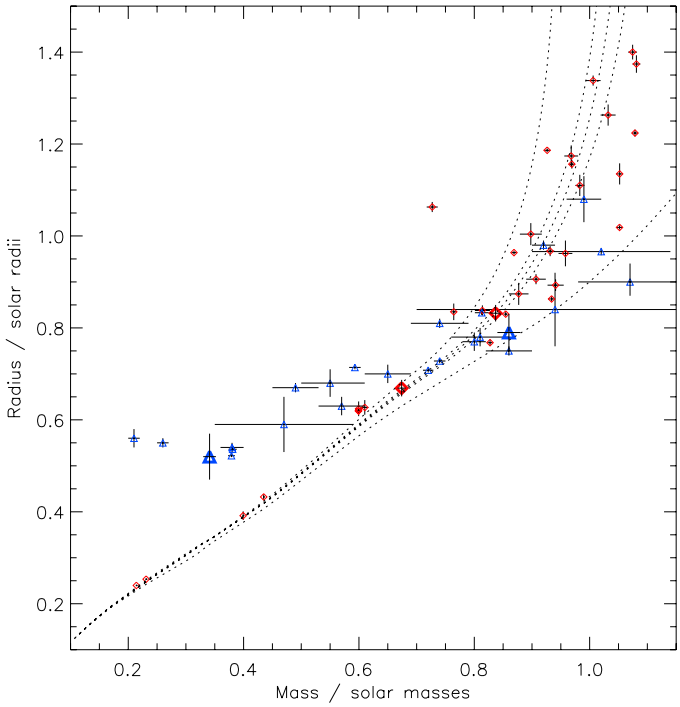

Fig. 23. Mass-radius diagram for binary components of J093010, compared with Dartmouth model isochrones for solar metallicity (dotted lines, corresponding to 1, 8, 9, 10 and 14 Gyr from bottom to top), and with empirical masses and radii for collected detached (red diamonds) and contact (blue triangles) eclipsing binary components. The binary components of J093010A are indicated by larger bold-face red diamonds, and those of J093010B by larger bold-face blue triangles.

An optimal average age of 10.3 ± 0.7 Gyr is indicated by this method. Then, plotting masses against radii, both components are consistent with solar metallicity isochrones between around 8 and 10 Gyr (Fig. 23); this implies an optimal average age of 9.2 ± 1.0 Gyr.

Figure 23 also shows that J093010A's binary components behave very similarly to Torres et al.'s collection of low-mass stars in detached eclipsing binaries with well-determined parameters (2010). The components of J093010B, however, do not sit on a single isochrone, presumably because of their interaction in contact: the primary has a smaller radius than its mass would imply, assuming an age of 9 or 10 Gyr, while the secondary's radius is much greater (and is inconsistent with any possible isochrone). Comparison with the parameters of short-period contact binary components collected by Stepień & Gazeas (2012), supplemented by two determined in Lohr et al. (2014a), suggests that this behaviour is entirely normal for systems of this configuration: all the secondaries (those with masses below 0.7 $M_{\odot}$) lie in this region of the mass-radius diagram, with clearly inflated radii, while the primaries in most cases have radii consistent with or even smaller than those expected from normal stellar evolution models.

5. Conclusion

After our initial discovery of J093010 as a probable doubly eclipsing quadruple system, and Koo et al.'s follow-up observations which confirmed J093010A as a double-lined spectroscopic binary and revealed the presence of a possible fifth component, we have carried out further spectroscopic and photometric observations of the whole system. We have confirmed J093010B as a double-lined spectroscopic binary also, and confirmed the association on the sky of the fifth component within J093010A. Radial velocities were measured for the first time for J093010B, allowing a more reliable determination of its mass ratio; the effective temperature of its primary, and of the assumed tertiary in J093010A, were also estimated from their disentangled individual spectra. Reanalysed SuperWASP photometry indicated the presence of a moving spot on one component of the binary in J093010A, with an apparent speed relative to its host star of approximately one rotation every two years.

After modelling both eclipsing systems we have obtained parameters for them which agree with those of Koo et al. in some areas, but disagree in several others, owing to different modelling approaches and available data. Specifically, we find a greater mass ratio for J093010B on the basis of our new spectroscopic data, and different radii for the binary components of J093010A as a result of our use of the total-annular eclipses in its light curves, which also allowed direct calculation of the third light contributed by the tertiary. Both binaries probably possess at least one large spot, though further observations would be required to constrain any spot properties plausibly.

On the basis of our temperature estimates from the disentangled component spectra, and from modelling, consistent distances for both binaries of 73 and 78 pc are found. The fifth non-eclipsing star appears to have a temperature and spectrum similar to those of the primaries in the two eclipsing binaries; a consistent distance is also found for it if it is assumed to be a typical main-sequence star. The system velocities of both binaries, and the average radial velocity of the fifth star, are all around −11 to −12 km s^{-1}. These findings strongly support the claim that both binaries, and very probably all five stars are gravitationally bound in a single system. The consistent angles of inclination of the two binary systems also imply likely formation by fragmentation from a single protostellar disk, without subsequent significant disruption to their orbital plane. The age of the system is around 9–10 Gyr, and it has approximately solar metallicity.

This bright, close, highly unusual star system, containing a very short-period contact eclipsing binary, and a triple system including a low-mass detached eclipsing binary, would doubtless repay further investigation.

Acknowledgements. The WASP project is currently funded and operated by Warwick University and Keele University, and was originally set up by Queen's University Belfast, the Universities of Keele, St. Andrews and Leicester, the Open University, the Isaac Newton Group, the Instituto de Astrofisica de Canarias, the South African Astronomical Observatory and by STFC. The *William Herschel* Telescope is operated on the island of La Palma by the Isaac Newton Group in the Spanish Observatorio del Roque de los Muchachos of the Instituto de Astrofisica de Canarias. This work was supported by the Science and Technology Funding Council and the Open University, and accomplished with the help of the VO-KOREL web service, developed at the Astronomical Institute of the Academy of Sciences of the Czech Republic in the framework of the Czech Virtual Observatory (CZVO) by P. Skoda and J. Fuchs using the Fourier disentangling code KOREL devised by P. Hadrava.

References

Batten, A. H., & Hardie, R. H. 1965, AJ, 70, 666
Cagaš, P., & Pejcha, O. 2012, A&A, 544, L3
Dotter, A., Chaboyer, B., Jevremović, D., et al. 2008, ApJS, 178, 89
Flower, P. J. 1996, ApJ, 469, 355
Graczyk, D., Soszyński, I., Poleski, R., et al. 2011, Acta Astron., 61, 103
Hadrava, P. 2012, in From Interacting Binaries to Exoplanets: Essential Modeling Tools, eds. M. T. Richards, & I. Hubeny, IAU, 351

Hilditch, R. W. 2001, An Introduction to Close Binary Stars (Cambridge: Cambridge University Press)
Holmes, S., Kolb, U., Haswell, C. A., et al. 2011, PASP, 123, 1177
Husser, T. O., von Berg, S. W., Dreizler, S., et al. 2013, A&A, 553, A6
Koen, C. 2014, MNRAS, 441, 3075
Kolb, U. 2014, in III Workshop on Robotic Autonomous Observatories, eds. J. C. Tello, A. Riva, D. Hiriart, & A. J. Castro-Tirado, Rev. Mex. Astron. Astrofis. Conf. Ser., 45, 16
Koo, J.-R., Lee, J. W., Lee, B.-C., et al. 2014, AJ, 147, 104
Lee, C. U., Kim, S. L., Lee, J. W., et al. 2008, MNRAS, 389, 1630
Lehmann, H., Zechmeister, M., Dreizler, S., Schuh, S., & Kanzler, R. 2012, A&A, 541, A105
Lohr, M. E., Norton, A. J., Kolb, U. C., et al. 2012, A&A, 542, A124
Lohr, M. E., Norton, A. J., Kolb, U. C., & Boyd, D. R. S. 2013a, A&A, 558, A71
Lohr, M. E., Norton, A. J., Kolb, U. C., et al. 2013b, A&A, 549, A86
Lohr, M. E., Hodgkin, S. T., Norton, A. J., & Kolb, U. C. 2014a, A&A, 563, A34
Lohr, M. E., Norton, A. J., Anderson, D. R., et al. 2014b, A&A, 566, A128
Norton, A. J., Payne, S. G., Evans, T., et al. 2011, A&A, 528, A90
Pollacco, D. L., Skillen, I., Cameron, A. C., et al. 2006, PASP, 118, 1407
Prša, A., & Zwitter, T. 2005, ApJ, 628, 426
Stepień, K., & Gazeas, K. 2012, Acta Astron., 62, 153
Torres, G., Andersen, J., & Giménez, A. 2010, A&AR, 18, 67
Wilson, R. E. 1994, International Amateur-Professional Photoelectric Photometry Communications, 55, 1
Wilson, R. E., & Devinney, E. J. 1971, ApJ, 166, 605

Table 1. Spectroscopic observations and heliocentric-corrected radial velocities for J093010.

HJD	Exp. time /s	(A) Prim. RV /km s^{-1}	δ Prim. RV	(A) Sec. RV	δ Sec. RV	(A) Ter. RV	δ Ter. RV	(B) Prim. RV	δ Prim. RV	(B) Sec. RV	δ Sec. RV
2 456 283.7679	5	87.5	1.0	−132.3	1.2	−11.8	0.5	28.9	1.5	−116.4	1.5
2 456 283.7704	30	90.1	0.7	−132.5	1.1	−11.1	0.6	40.4	1.5	−138.1	1.5
2 456 283.7710	30	88.6	1.6	−133.0	1.3	−11.1	0.3	39.2	1.5	−143.4	1.5
2 456 283.7716	30	89.7	0.6	−130.9	0.5	−11.3	0.9	44.5	1.5	−141.7	1.5
2 456 283.7749	180	88.3	0.5	−133.3	0.9	−11.4	0.6	51.5	1.5	−162.8	1.5
2 456 283.7773	180	88.7	0.8	−133.2	0.3	−11.0	0.3	52.6	1.5	−179.0	1.5
2 456 283.7796	180	88.4	0.4	−133.3	0.3	−10.98	0.25	55.9	1.5	−180.8	1.5
2 456 283.7853	360	89.1	0.4	−133.0	0.8	−11.2	0.8	69.2	1.5	−203.4	1.5
2 456 283.7897	180	89.0	0.5	−133.4	1.2	−11.5	0.4	71.1	1.5	−219.4	1.5
2 456 283.7921	180	88.7	0.3	−133.0	0.9	−10.58	0.14	74.1	1.5	−237.1	1.5
2 456 283.7979	360	86.8	1.0	−134.2	2.0	−13.0	1.6				
2 456 292.7661	60	58.01	0.18	−102.3	1.5	−12.35	0.18	−64.6	1.5	124.7	1.5
2 456 292.7671	60	60.3	0.7	−101	3	−12.3	0.6	−63.3	1.5	125.4	1.5
2 456 292.7680	60	59.0	0.6	−99.6	1.3	−11.8	0.5	−66.7	1.5	132.3	1.5
2 456 292.7710	10	58.8	1.6	−98	5	−13.3	1.1	−79.4	1.5	147.3	1.5
2 456 292.7743	10	55.9	1.3	−102.5	2.2	−13.1	0.3	−84.1	1.5	163.5	1.5
2 456 292.7758	60	59.4	0.8	−106.4	0.8	−13.39	0.19	−88.6	1.5	170.3	1.5
2 456 292.7767	60	59.7	0.8	−106.1	2.5	−13.1	0.5	−88.7	1.5	173.2	1.5
2 456 292.7777	60	59.33	0.12	−107.54	0.18	−14.3	0.7	−93.9	1.5	176.0	1.5
2 456 292.7822	360	61.2	0.5	−106.6	0.4	−13.2	0.4	−100.4	1.5	197.7	1.5
2 456 292.7866	360	62.5	0.6	−107.6	0.5	−13.2	0.5	−107.0	1.5	213.8	1.5
2 456 292.7911	360	63.8	0.4	−110.5	0.7	−13.16	0.18	−109.8	1.5	229.5	1.5
2 456 292.7948	60	67.2	1.5	−113.0	0.6	−16.8	1.8	−118.7	1.5	237.3	1.5
2 456 292.7957	60	68.8	2.3	−110.2	0.6	−10.9	0.7	−116.4	1.5	239.8	1.5
2 456 292.7967	60	69.3	0.8	−112.5	0.9	−12.8	0.9	−114.4	1.5	246.6	1.5
2 456 292.7992	300	66.4	0.7	−112.4	0.8	−13.6	0.4	−116.0	1.5	247.1	1.5
2 456 292.8029	300	67.7	0.4	−112.2	0.9	−12.83	0.13	−119.0	1.5	247.5	1.5
2 456 292.8066	300	68.49	0.06	−114.9	0.9	−13.1	0.3	−117.5	1.5	247.6	1.5
2 456 294.7665	60	−91.7	0.8	96.0	1.7	−9.05	0.13	67.1	1.5	−209.4	1.5
2 456 294.7674	60	−91.4	1.4	96.3	2.2	−9.1	0.3	66.6	1.5	−196.4	1.5
2 456 294.7684	60	−93.6	0.6	94.4	1.1	−9.6	0.5	64.0	1.5	−197.0	1.5
2 456 294.7707	120	−94.4	0.6	94.9	0.9	−10.25	0.10	67.8	1.5	−178.5	1.5
2 456 294.7724	120	−94.4	0.7	95.9	0.3	−9.67	0.15	58.6	1.5	−179.1	1.5
2 456 294.7740	120	−95.4	0.4	95.7	0.4	−10.40	0.06	56.1	1.5	−171.7	1.5
2 456 294.7783	110	−95.59	0.14	97.0	1.2	−10.07	0.21	45.0	1.5	−143.4	1.5
2 456 294.7799	110	−97.0	0.4	96.4	1.1	−10.8	0.5	37.4	1.5	−143.4	1.5
2 456 294.7814	110	−96.6	0.5	96.6	1.2	−10.22	0.20	37.4	1.5	−126.2	1.5
2 456 294.7829	110	−97.8	0.3	96.7	0.3	−10.69	0.09	32.7	1.5	−128.3	1.5
2 456 294.7845	110	−97.2	0.4	98.1	0.6	−10.2	0.3	31.0	1.5	−108.3	1.5
2 456 294.7860	110	−98.2	0.5	96.9	1.5	−10.85	0.08	19.9	1.5	−95.7	1.5
2 456 294.7885	110	−99.0	0.4	96.5	0.7	−11.03	0.12	13.6	1.5	−76.9	1.5
2 456 294.7901	110	−99.2	1.0	97.3	1.0	−11.02	0.24	13.5	1.5	−73.1	1.5
2 456 294.7916	110	−98.8	0.4	97.8	1.0	−10.53	0.21	7.9	1.5	−56.5	1.5
2 456 294.7931	110	−100.02	0.16	96.9	0.4	−11.25	0.24	−1.4	1.5	−41.4	1.5
2 456 294.7947	110	−99.4	0.4	98.3	0.8	−10.61	0.22	−2.3	1.5	−35.0	1.5
2 456 294.7962	110	−100.3	0.4	97.7	1.4	−11.39	0.20	−5.2	1.5	−29.5	1.5
2 456 294.7986	60	−99.7	0.6	100.5	1.3	−10.5	0.6	−16.1	1.5	−3.7	1.5
2 456 294.7996	60	−100.5	1.1	98.7	1.6	−10.8	0.3	−10.2	1.5	−20.6	1.5
2 456 294.8005	60	−102.0	0.7	99.6	0.5	−11.9	0.3	−17.3	1.5	−5.8	1.5